Omnidirectional Harvesting of Weak Light Using a Graphene Quantum Dot-Modified Organic/Silicon Hybrid Device

Meng-Lin Tsai[†∥], Dung-Sheng Tsai[†#∥], Libin Tang[§], Lih-Juann Chen[*‡], Shu Ping Lau[§], and Jr-Hau He[*†]

[†] Computer, Electrical and Mathematical Sciences and Engineering (CEMSE) Division, King Abdullah University of Science and Technology (KAUST), Thuwal 23955-6900, Kingdom of Saudi Arabia

[‡] Department of Materials Science and Engineering, National Tsing Hua University, Hsinchu 30013, Taiwan, Republic of China

[#] Institute of Photonics and Optoelectronics & Department of Electrical Engineering, National Taiwan University, Taipei 10617, Taiwan, Republic of China

[§] Department of Applied Physics, The Hong Kong Polytechnic University, Hung Hom, Kowloon, Hong Kong SAR

DOI: 10.1021/acsnano.6b08567

Publication Date (Web): April 21, 2017

*E-mail: jrhau.he@kaust.edu.sa., *E-mail: ljchen@mx.nthu.edu.tw.

Abstract

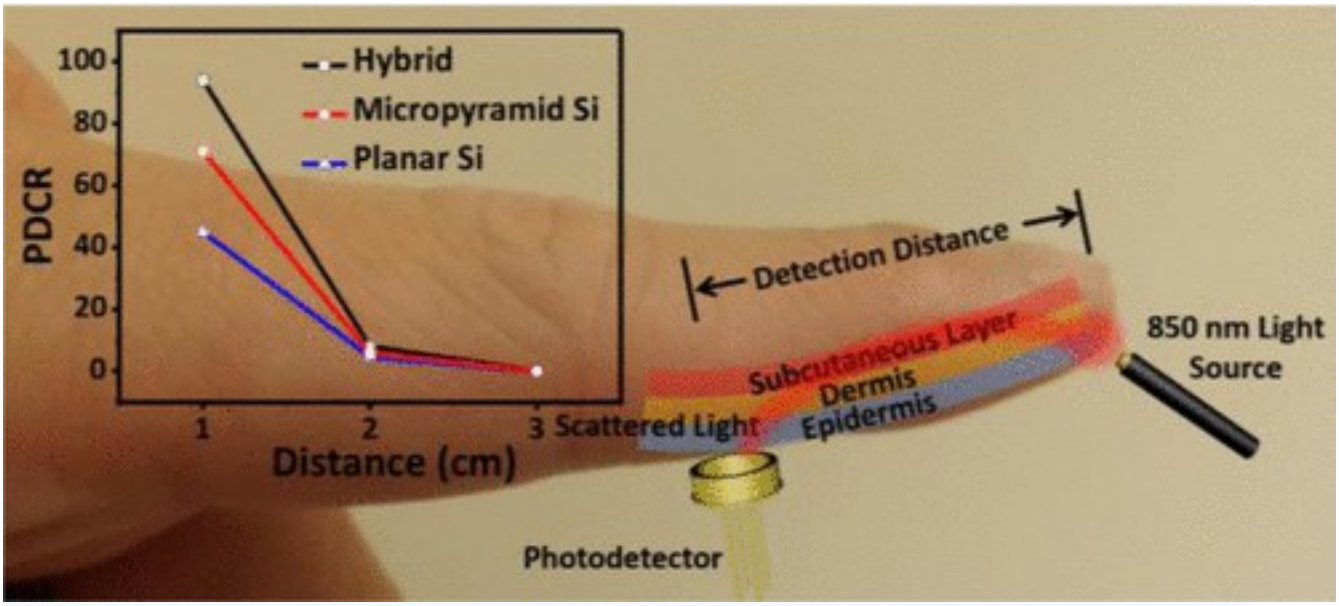

Despite great improvements in traditional inorganic photodetectors and photovoltaics, more progress is needed in the detection/collection of light at low-level conditions. Traditional photodetectors tend to suffer from high noise when operated at room temperature; therefore, these devices require additional cooling systems to detect weak or dim light. Conventional solar cells also face the challenge of poor light-harvesting capabilities in hazy or cloudy weather. The real world features such varying levels of light, which makes it important to develop strategies that allow optical devices

to function when conditions are less than optimal. In this work, we report an organic/inorganic hybrid device that consists of graphene quantum dot-modified poly(3,4-ethylenedioxythiophene) polystyrenesulfonate spin-coated on Si for the detection/harvest of weak light. The hybrid configuration provides the device with high responsivity and detectability, omnidirectional light trapping, and fast operation speed. To demonstrate the potential of this hybrid device in real world applications, we measured near-infrared light scattered through human tissue to demonstrate noninvasive oximetric photodetection as well as characterized the device's photovoltaic properties in outdoor (*i.e.*, weather-dependent) and indoor weak light conditions. This organic/inorganic device configuration demonstrates a promising strategy for developing future high-performance low-light compatible photodetectors and photovoltaics.

Keywords:
graphene quantum dots; **hybrid**; **omnidirectional**; **PEDOT:PSS**; **weak light**

In photodetection and photovoltaic applications, the pursuit of weak and omnidirectional light detection/harvest has become one of the major goals in developing next-generation photo-optical devices.(1-3) For example, traditional photodetectors (PDs) tend to have high noise under low-light conditions that are often typical of imaging and biosensing applications.(4) For developing high-performance optical communication devices, it is also important to design PDs with omnidirectional and weak light detectors in order to increase the sensitivity and signal quality.(5)Under an overcast sky, over 90% of the total incident solar radiation is diffused through the cloud layer, so it cannot be successfully harvested, limiting the efficiency of solar cells.(6) To improve the practicality of these technologies, it is essential to develop a strategy that enables these devices to perform well even under omnidirectional and low-light conditions.

For the past several decades, inorganic PDs have dominated applications in photodetection. For example, GaN-, Si-, and InGaAs-based PDs have been used to detect ultraviolet (250–400 nm), visible (450–800 nm), and infrared (900–1700 nm) wavelengths of light, respectively.(4) In recent years, researchers have successfully fabricated various types of inorganic PDs for different functions, such as atomically thick 2D devices with omnidirectional detection and ultrahigh gain, and Ga_2O_3/SiC-based materials for harsh electronics and transparent solar-blind detection.(7-11)However, in order to increase the sensitivity and reduce noise levels, particularly for low-light conditions, a cooling system is usually required, which increases the cost and complexity of the inorganic PD design.(12) In addition, inorganic PDs often require a high operation voltage and have limited ranges of wavelengths that they can detect, which hampers the practical application of these technologies. Nanostructure-based PDs, such as those that use CdS and PbS quantum dots, have

demonstrated ultrahigh sensitivity with low power consumption in weak light environments.(13, 14) However, the fabrication of Cd- and Pb-based quantum dots requires toxic materials and is therefore not a sustainable solution.

To satisfy the requirements for future communication, image- and biological-sensing applications, broadband and high-detectivity PDs are needed that are also low-cost, operate at low-voltage, and can detect weaker sources of light without the need for a cooling system. Many researchers have turned to organic-based PDs to achieve these aims. For example, Gong *et al*. reports an organic PD design that demonstrates performance comparable to inorganic PDs by using a multilayer polymer structure that helps reduce the dark current noise for detectivities of up to 10^{12} Jones as well as a wide spectral response from 300 to 1450 nm.(4) Solution-processed organic–inorganic hybrid perovskite materials have also been used to develop PDs with high detectivity.(15-17)

However, the response time of organic-based PDs is usually longer than that of inorganic ones due to the lower carrier mobilities of organic materials. Moreover, the faster charge carriers in organic PDs must wait for the slower charge carriers at the interface before recombination, which further limits the response time of the device.(18) In addition, the detectivity of organic-based PDs is still relatively low in certain wavelength regions.(4, 15-17) In previous work, we have proposed a promising method of using a graphene quantum dot (GQD)-modified organic layer to achieve concurrent improvement in optical and electrical properties in order to simultaneously increase the mobility and light trapping capability of the organic layer. The photon downconversion behavior of the GQD can be utilized to harvest additional ultraviolet photons to improve the absorption of the device. In the meantime, the highly conductive GQD also improves the conductivity of the organic layer.(19)

For photovoltaic devices, researchers have applied various photon management techniques that enable omnidirectional and weak light harvesting, such as hierarchical surface engineering, graded refractive index antireflective coatings, and the employment of colloidal nanospheres or periodic nanopillar arrays.(20-24) However, these omnidirectional light-harvesting methods are often achieved using complex fabrication processes, which usually come with unwanted defects, recombination sites, and contaminations that deteriorate the device's performance and thus require additional treatment procedures.(20-24) To overcome these issues, we need to develop simpler techniques, such as solution processing, to construct devices that enable omnidirectional harvesting of light under outdoor and indoor low-light conditions. Recently, we used GQD-poly(3,4-ethylenedioxythiophene) polystyrenesulfonate (PEDOT:PSS) to increase the surface morphology, conductivity, and electrocatalytic activity in Pt-free dye-sensitized solar cells for achieving weak light

harvesting.(1) The device shows extraordinarily superior performance under indoor and outdoor weak light conditions, providing an economical solution for weak light harvesting in dye-sensitized solar cells.

Pure inorganic devices usually perform well at normal to high light power (such as at noon of a sunny day when the power density is close to or over 100 mW/cm^2), while pure organic devices are good at weak light (such as at dawn, sunset, or cloudy days when the power density is <100 mW/cm^2). To develop omnidirectional PDs and photovoltaics that function at normal- to low-light levels, we have combined the advantages of inorganic (*i.e.*, stability and high speed) and organic materials (*i.e.*, low-cost and facile solution-processing) into a single device. By dispersing GQD in a PEDOT:PSS solution that was subsequently spin-coated on a microtextured Si substrate, we were able to fabricate high-detectivity PDs and photovoltaic devices that demonstrated excellent omnidirectional light-harvesting capability, even at weak light conditions. Compared with planar Si PDs, the detectivity and responsivity of our hybrid PD device exhibited a ~3-fold enhancement under 532 nm illumination at a light power of 25.2 μW. At large angles of incidence (AOIs), our hybrid device exhibited more than 2.5-fold enhancement in responsivity compared to the planar Si PD control, demonstrating this technology's potential for omnidirectional light-detection applications. We performed real-world-type measurements using this hybrid device, including photodetection of near-infrared light scattered through human tissue, which is widely used for noninvasive oximetric measurements,(25) as well as photovoltaic characterization in outdoor weather-dependent and indoor weak light conditions. We show that the hybrid device exhibits a far superior photo-to-dark-current ratio (PDCR) compared to that of planar Si PDs used in human finger tissue measurements, demonstrating an over 2-fold PDCR enhancement when the scattered light is detected at 1 cm from the light source. In addition, in real-world weak light photovoltaic measurements, the hybrid device had an enhanced fill factor (FF) in all weak light conditions, resulting in better power conversion efficiency (PCE) than that of planar Si solar cells. Accordingly, the high-detectivity, low-cost, and omnidirectional properties of these hybrid devices, along with their practical real-world compatibility, provide possibilities for the next generation of photosensing, bioimaging, and energy-harvesting applications.

Results and Discussion

Our design concept is to combine organic (PEDOT:PSS) and inorganic (Si) materials in order to achieve high performance from weak light to strong light conditions. We have previously

demonstrated that the incorporation of GQD can effectively enhance the performance of our Si/PEDOT:PSS hybrid device due to concurrent improvement of electrical and optical properties; GQD can improve the conductivity of PEDOT:PSS film, and its downconversion behavior can be used to enhance light absorption in the short wavelength region.(19) We also adopted the design in this study in order to make our device more competitive under various light conditions. First, we began by fabricating a micropyramidal textured surface on the top of an n-type Si substrate using a chemical etching process, as shown in Figure 1a.(6) The detailed fabrication procedure is provided in the Methods section. Such microfeatures (~10 μm) have been shown to improve the harvesting efficiency of incident broadband, omnidirectional photons.(6)

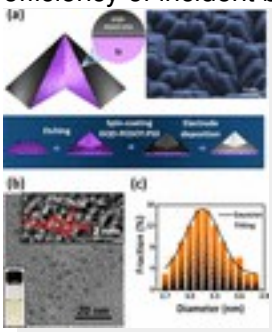

Figure 1. (a) The schematic, SEM image, and fabrication process of the hybrid device. (b) TEM and high-resolution TEM (inset) images of the GQDs and a photograph of the GQD solution. (c) The diameter distribution of the sampled GQDs (~100) as measured from TEM images. The black line in (c) is the Gaussian fitting curve.

Next, we synthesized GQDs by microwave-assisted annealing of glucose in a deionized water solution.(26) We used transmission electron microscopy (TEM) to characterize the size and distribution of the as-prepared GQDs, as indicated in Figure 1b. A high-resolution TEM image shows the enlarged structure of a single GQD, which exhibits 0.213 nm fringes that correspond to the *d* spacing between the graphene layers (inset of Figure 1b).(27) A photographic image of the GQDs in deionized water has also been provided to demonstrate the pale-yellow color of the suspension as a result of GQD formation.(26) We measured the size distribution of the GQDs from TEM images (Figure 1c) and determined that the average size was 3.2 nm, which corresponds to ~10 layers of graphene in each QD. In addition, the full-width-at-half-maximum of the fitted Gaussian curve of the size distribution was 0.5 nm, demonstrating that we can well control the size of the GQDs by adjusting the annealing time. The as-prepared GQDs were added to a commercial PEDOT:PSS solution and then spin-coated on the micropyramidal-structured Si substrate and annealed in a N_2-rich glovebox at 165 °C for 10 min. Ag and Al contact electrodes were thermally evaporated on the top and back sides of the sample, respectively, to form the hybrid PD device.

Commercially available micropyramidal and planar Si solar cells with SiN_x antireflective layers were used as controls in our experiments.

As shown in Figure 2a, we measured the *I*–*V* characteristics of the hybrid PD in the dark and under 532 nm illumination at different powers and an AOI of 0°. To compare with conventional devices, we also characterized the control micropyramidal and planar Si devices, as shown in Figure 2b,c, respectively. Under 532 nm illumination and at power intensities above 25.2 μW, all three devices exhibited similar photocurrents within a voltage range from −1 to 0.75 V. However, the dark current of the hybrid PD was an order of magnitude smaller than that of the two control PDs, especially near 0 V, demonstrating a significantly low level of noise for low-light conditions (<1 mW). The low noise level can be attributed to the fact that the PEDOT:PSS material is an ideal electron blocking layer that can effectively prevent unwanted hot carriers from reaching the top electrode, even at room temperature. For conventional (*i.e.*, inorganic) PDs, increased sensitivity of the device at low-light levels is usually achieved with the aid of a cooling system.

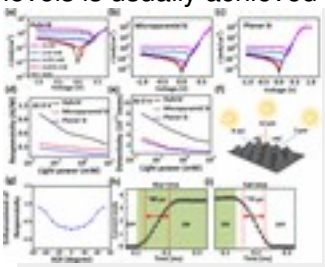

Figure 2. (a–c) Current–voltage characteristics of the hybrid, micropyramidal Si, and planar Si PDs measured in the dark and under 532 nm illumination with varying light power intensity. (d, e) The 532 nm laser intensity-dependent (d) responsivity and (e) detectivity of the hybrid, micropyramidal Si, and planar Si PDs measured at 0 V. (f) Schematic of angular-dependent photodetection of the sun. (g) Enhancement of responsivity of the hybrid PDs measured at 0 V under 850 nm light. (h, i) The rise and fall time of the hybrid PDs measured at 0 V under 850 nm light illumination.

Because the hybrid PD has low noise, it also exhibited the highest responsivity for a power intensity below 1 mW among all three PD devices, as indicated in Figure 2d. At 2.52 μW, the responsivity of the hybrid PD increased to 1.02 A/W, which is about 57-fold higher than recently published results for PEDOT:PSS/Si devices (∼18 mA/W).(28) This suggests that our hybrid PD would be superior for self-powered (since the responsivity can be measured at zero bias), low-light photosensing applications. For low-light PD characterization, the noise equivalent power (NEP) is usually calculated with eq 1:

$$\mathrm{NEP} = (A\Delta f)^{1/2}/D^{*} \quad (1)$$

where A is the effective area of the detector in cm^2, Δf is the electrical bandwidth in Hz, and D^* is the detectivity measured in units of Jones, which can be calculated with eq 2:

$$D^{*} = R/(2qJ_{\mathrm{d}})^{1/2} \quad (2)$$

where R is the responsivity in A/W, q is the absolute

value of the electron charge, and J_d is the dark current. At zero bias, the calculated detectivity of the hybrid PD increased from 3 × 10^{11}Jones to 8 × 10^{11} Jones as the power intensity decreased from 8 mW to 25.2 μW, as shown in Figure 2e. The detectivity at 25.2 μW is 2 times of the recently reported result for the PEDOT:PSS/Si device (4.1 × 10^{11} Jones).(28) The self-powered, cooling system-free, and low-light detection properties of these hybrid PDs are expected to be well-suited for ultralow power, room temperature, and ultrasensitive biological imaging applications, which will be demonstrated later in this work.

However, in real-world photodetection and photovoltaic applications, light can be incident from all directions. For example, the angle at which sunlight strikes the earth varies across the day as indicated in Figure 2f. Therefore, we characterized the AOI-dependent photodetection properties of the hybrid, micropyramid Si, and planar Si PDs (Figure S1). Since scattered infrared radiation is typically used in optical communications(4) and clinical applications, such as to monitor a patient's blood oxygen levels using an oximeter,(29) we used 850 nm light for this AOI-dependent characterization experiment. The responsivity of the hybrid PD was enhanced for all AOIs studied (0° to 75°) compared with the micropyramid and planar Si PD. The enhanced responsivity of the hybrid PD was further revealed by calculating the enhancement (E_R) of the hybrid PD with respect to the micropyramid Si PD device according to eq 3:

$$E_R = \frac{R_{hybrid} - R_{Si}}{R_{Si}} \quad (3)$$

where R_{hybrid} and R_{Si} are the responsivities of the hybrid and micropyramid Si PDs, respectively. As shown in Figure 2g, the enhancement of the responsivity of the hybrid PD was up to 0.9 as compared with the micropyramid Si PD under high AOIs (±75°), demonstrating that the hybrid device has excellent omnidirectional photodetection properties. We have demonstrated in our previous work that by incorporating 0.5 wt % of GQDs, the resistivity of the PEDOT:PSS film can be improved from 9.6 × 10^{-4} to 1.5 × 10^{-4} Ω·cm.(19) Moreover, it has been demonstrated previously that in addition to downconversion effect, GQDs also exhibit upconversion effect under long wavelength.(30, 31) Shen *et al*. demonstrated excitation-dependent upconversion emission of GQDs. The emission peaks changed from 390 to 468 nm as the excitation wavelength changed from 600 to 800 nm, respectively. The underlying mechanism for the upconversion properties of GQDs can be originated to the multiphoton active process and anti-Stokes transition. Therefore, the long wavelength enhancement can be attributed to the combined effect of improved conductivity and upconversion effect of GQDs. At high AOIs, the penetration depth of the light decreases so that light could be scattered or reflected before reaching the active region of micropyramid Si. As the thickness of PEDOT:PSS layer is only ∼30 nm with very high transmittance, light with high AOI can be effectively absorbed at the PEDOT:PSS/Si interface.

Therefore, the responsivity enhancement can be more significant at high AOI. We also characterized the temporal resolution of the hybrid PD in terms of the rise and fall times of the photoresponse, which were ∼80 μs and ∼70 μs as indicated in Figure 2h,i, respectively. Typically, the carrier mobility of organic materials is much slower than that of inorganic materials, resulting in a slow reaction time. However, by using a Si substrate with only a ∼30 nm-thick GQD-PEDOT:PSS layer deposited on its surface, the response time of the device was retained due to the fast operation time of the Si. The response time of the micropyramidal Si PD is also characterized and shown in Figure S2 of the Supporting Information. Therefore, using an organic/Si hybrid design enabled us to achieve low-cost, omnidirectional, and high-detectivity photodetection without sacrificing the temporal resolution of the device.

To demonstrate a real-world case, we designed an oximetry-like experiment to detect infrared light propagated/scattered through human finger tissue, as shown in Figure 3a. As infrared light enters the tissue, it encounters epidermis, dermis, and subcutaneous layers, generating ballistic, quasi-ballistic, and diffuse photons. The intensities of the ballistic and quasi-ballistic photons are high. However, for concentrated tissue media, these types of photons are scarce, and their interaction with biological tissue is weak, leading to poor resolution. Therefore, diffuse photons are preferred for biological imaging.(25) Since diffuse photons interact strongly with the surrounding tissue, their intensity is usually weak, and the incident angle to the PD is high, and thus omnidirectional, low-light PDs are required. We measured the *I*–*V* characteristics of the hybrid PD at different detection distances (Figure S3). The detection distance is defined as the length between the light source and the PD shown in Figure 3a, with larger distances resulting in a weaker signal. As shown in Figure 3b, the self-powered hybrid PD exhibited enhanced PDCR as compared with micropyramid and planar Si PDs for a detection distance shorter than 3 cm at 0 V. The PDCR of the hybrid PD at a detection distance of 1 cm was nearly 100, which was twice as much compared to the planar Si PD. Accordingly, the self-powered hybrid PD showed excellent low-light and omnidirectional photon collection capability, which demonstrates its effectiveness for low-light level biological imaging applications.

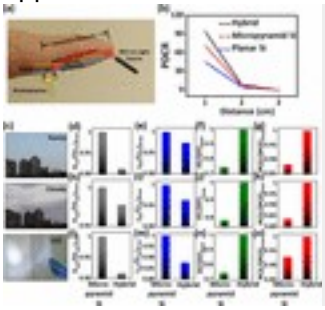

Figure 3. (a) Schematic of the detection of 850 nm light propagating through human finger tissue. (b) PDCR of the PDs as a function of the 850 nm light propagation distance through human finger tissue. The light intensity (I_{light}) was 3×10^3 W/m^2. (c) Photographic images of the real-world low-light measurement conditions. (d–o) Comparison between the micropyramidal Si and hybrid devices in terms of their maximum V_{OC}, J_{SC}, FF, and PCE photovoltaic parameters on (d–g) a sunny day (condition (i)), (h–k) a cloudy day (condition (ii)), and (l–o) under an LED with a power density of 3.5 mW/cm^2 (condition (iii)).

The hybrid PD exhibits self-powered, omnidirectional, and low-light detection properties. These intriguing characteristics are also desired for next-generation photovoltaic devices. In the past several years, researchers have reported omnidirectional PEDOT:PSS/Si hybrid solar cells with efficiencies as high as 11% using hierarchical surface engineering (*e.g*, nanowires on micropyramids) and thin oxide passivation strategies.(6) Moreover, solution processing offers the possibility of employing chemical additives, such as quantum dots, in order to expand the absorption of solar cells to the UV region.(6) Despite the development of organic/inorganic hybrid solar cells as more cost-effective devices, researchers have typically neglected their underlying potential at low-light conditions. In the *I*–*V* curves shown in Figure 1a, we observed that the hybrid device features a photocurrent at 0 V, which indicates photovoltaic behavior. Additionally, the spectral responsivity of the three devices at 0 V is shown in Figure S4. Compared to the planar Si device, the micropyramidal Si and hybrid devices show enhanced spectral responsivity throughout the range of wavelengths of solar irradiance due to superior photon management by the micropyramidal surface that was shared on both devices as well as the concurrent improvement of the optical and electrical properties of the hybrid device by the GQD additive in the PEDOT:PSS layer.(19) It is expected that under 1 sun AM 1.5G solar irradiation, the photovoltaic performance of the Si solar cells will be superior to that of the hybrid device (Figure S5). However, for low-light conditions, surface and bulk recombinations in the Si become more serious due to unfilled defects, resulting in decreased FF values. In contrast, for the hybrid device, the PEDOT:PSS layer is an efficient hole transporting (*i.e.*, electron blocking) material. Therefore, we expect that for low-light conditions, the FF of the hybrid device could increase tremendously.

To demonstrate real-world low-light conditions, we measured the hybrid device under three light settings (Figure 3c) and compared the results with the micropyramidal Si device (Figures S6–S8). The three conditions included: (i) an outdoor measurement on a sunny day (17:30); (ii) an outdoor measurement on a cloudy day (13:00); and (iii) an indoor light-emitting diode (LED) measurement with a power density of 3.5 mW/cm^2. The comparisons of the open-circuit voltage (V_{OC}), short-circuit current (J_{SC}), FF, and PCE of the hybrid and micropyramidal Si devices measured under conditions

(i), (ii), and (iii) are shown in Figure 3d–g, h–k, and l–o, respectively. The maximum value indicated in these figures is the highest value for each photovoltaic parameter (V_{oc}, J_{sc}, FF, and PCE) at each condition (sunny, cloudy, and indoor). Under these three low-light conditions, the micropyramidal Si device had higher V_{oc} and J_{sc} values. However, the hybrid device showed significantly higher FF for all three conditions, leading to higher PCE values overall. These real-world tests demonstrate that due to the omnidirectional and low-light harvesting characteristics of the hybrid device, it showed impressive photovoltaic performance and thus could be competitive in the solar marketplace.

Conclusion

In summary, the hybrid device made using a GQD-PEDOT:PSS/Si configuration has been demonstrated to be highly effective for low-light applications in photodetection and photovoltaics due to its self-powered, low-noise, high-detectivity, omnidirectional, and high-speed properties, which could not otherwise be achieved using an inorganic or organic semiconductor device alone. Under 532 nm illumination, the detectivity of the GQD-PEDOT:PSS/Si hybrid device was as high as 8×10^{11} Jones without the application of a bias voltage. We also performed infrared low-light detection at 850 nm to demonstrate the capability of this device for high-speed optical communication and biological imaging applications. In addition, we characterized photovoltaic behavior using outdoor weather dependent and indoor weak light conditions to demonstrate the superior PCE of the hybrid cells in all weak light conditions *via* an enhanced FF due to efficient hole transport (*i.e.*, electron blocking) of the PEDOT:PSS layer, as compared to all-inorganic Si solar cells. We believe the combination of these properties in the hybrid device meet real-world requirements and therefore holds promise for the application of this technology in biological imaging and low-light energy generation and photodetection.

Methods

Preparation and Characterization of Micropyramidal Structured Si

Monocrystalline n-type (100) Si wafers (E-Light Technology Inc.) with a resistivity of 5–10 Ω-cm were immersed in an isotropic etching solution consisting of potassium hydroxide (Sigma-Aldrich, > 98%), isopropyl alcohol (Sigma-Aldrich, > 99.5%), and H_2O with a volume ratio of 1:1:17 at 85 °C for 20 min. Scanning electron microscopy (SEM) measurements were performed on a JEOL JSM-7100F microscope at an operation voltage of 15 kV.

Synthesis and Characterization of GQD

First, we prepared an 11.1 wt % glucose solution in deionized water. Then we siphoned ∼2.5 mL of that solution into a glass bottle and tightly closed it. The glass bottle was heated with a conventional microwave oven at 600 W for 5 min. The microwave power, heating time, concentration, and solution volume can be adjusted to control the size of the GQD.(26) During the microwave heating process, the solution changes in color from transparent to pale yellow as a result of the formation of GQD. Subsequently, the glass bottle was cooled to room temperature for characterization. TEM measurements were performed on a JEOL JEM-2100F microscope at an operation voltage of 200 kV.

Preparation of the Hybrid Device

Commercially available PEDOT:PSS solution (PH 500, Clevios) was used with 5 wt % dimethyl sulfoxide (Sigma-Aldrich, > 99.9%) and 0.1 wt % Triton X-100 surfactant (Sigma-Aldrich) as intrinsic additives. 0.5 wt % GQD solution was added to this PEDOT:PSS mixture, and the resulting GQD-PEDOT:PSS material was subsequently spin-coated on the micropyramidal structured Si substrate and annealed in a N_2-rich glovebox at 165 °C for 10 min. Finally, Ag and Al contact electrodes were thermally evaporated under vacuum in homemade thermal evaporators on the top and back sides of the sample, respectively, to form the hybrid device.

Device Measurements

Electrical measurements were carried out on a probe-station and measured with an Agilent B2902A sourcemeter, along with a 532 nm laser (diode-pumped crystal laser from Onset Electro-Optics Co.) and 850 nm LED (Thorlabs) illumination. The AOI-dependent measurements were completed by adjusting the angle of the sample stage with a protractor. The spectral responses were measured using an Enlitech QE-R spectal response system. The photodetection of light scattered through human tissue was performed by placing the 850 nm light source and the PD at a specified distance apart along a human fingertip. The PD was packaged using copper wire connected to the source meter and silver paste and covered with glass slides. Photovoltaic characterization was carried out by placing the device in an outdoor open space or under an LED with a power density of 3.5 mW/cm^2. The outdoor conditions included: (i) a sunny day, which occurred at 25°1′7″ N and 121°32′31″ E at 17:30 on April 26th, 2014; and (ii) a cloudy day, which occurred at 25°1′7″ N and 121°32′31″ E at 13:00 on April 27th, 2014.

Acknowledgment

This research was supported by KAUST baseline funding, the Research Grants Council of Hong Kong (Project no. PolyU 153012/14P) and National Natural Science Foundation of China (NSFC grant no. 11374250).

- Reference QuickView
-

References

This article references 31 other publications.

1. 1.

Lee, C. P.; Lin, C. A.; Wei, T. C.; Tsai, M. L.; Meng, Y.; Li, C. T.; Ho, K. C.; Wu, C. I.; Lau, S. P.; He, J. H.Economical Low-Light Photovoltaics by Using the Pt-Free Dye-Sensitized Solar Cell with Graphene Dot/PEDOT:PSS Counter Electrodes *Nano Energy* **2015**, 18, 109– 117 DOI: 10.1016/j.nanoen.2015.10.008

[Crossref], [CAS]

2. 2.

Steim, R.; Ameri, T.; Schilinsky, P.; Waldauf, C.; Dennler, G.; Scharber, M.; Brabec, C. J. Organic Photovoltaics for Low Light Applications *Sol. Energy Mater. Sol. Cells* **2011**, 95, 3256– 3261 DOI: 10.1016/j.solmat.2011.07.011

[Crossref], [CAS]

3. 3.

Chen, C. Y.; Chang, J. H.; Chiang, K. M.; Lin, H. L.; Hsiao, S. Y.; Lin, H. W. Perovskite Photovoltaics for Dim-Light Applications *Adv. Funct. Mater.* **2015**, 25, 7064– 7070 DOI: 10.1002/adfm.201503448

[Crossref], [CAS]

4. 4.

Gong, X.; Tong, M.; Xia, Y.; Cai, W.; Moon, J. S.; Cao, Y.; Yu, G.; Shieh, C. L.; Nilsson, B.; Heeger, A. J.High-Detectivity Polymer Photodetectors with Spectral Response from 300 to 1450 nm *Science* **2009**, 325,1665– 1667 DOI: 10.1126/science.1176706

[Crossref], [PubMed], [CAS]

5. 5.

Zhang, X.; Tang, Y.; Huang, H.; Zhang, L.; Bai, T. Design of an Omnidirectional Optical Antenna for Ultraviolet Communication *Appl. Opt.* **2014**, 53, 3225– 3232 DOI: 10.1364/AO.53.003225

[Crossref], [PubMed], [CAS]

6. 6.

Wei, W. R.; Tsai, M. L.; Ho, S. T.; Tai, S. H.; Ho, C. R.; Tsai, S. H.; Liu, C. W.; Chung, R. J.; He, J. H. Above-11%-Efficiency Organic-Inorganic Hybrid Solar Cells with Omnidirectional Harvesting Characteristics by Employing Hierarchical Photon-Trapping Structures *Nano Lett.* **2013**, 13, 3658– 3663 DOI: 10.1021/nl401540h

[ACS Full Text], [CAS]

7. 7.

Tsai, D. S.; Liu, K. K.; Lien, D. H.; Tsai, M. L.; Kang, C. F.; Lin, C. A.; Li, L. J.; He, J. H. Few-Layer MoS_2 with High Broadband Photogain and Fast Optical Switching for Use in Harsh Environments *ACS Nano* **2013**, 7,3905– 3911 DOI: 10.1021/nn305301b

[ACS Full Text], [CAS]

8. 8.

Wei, T. C.; Tsai, D. S.; Ravadgar, P.; Ke, J. J.; Tsai, M. L.; Lien, D. H.; Huang, C. Y.; Horng, R. H.; He, J. H.See-Through Ga_2O_3 Solar-Blind Photodetectors for Use in Harsh Environments *IEEE J. Sel. Top. Quantum Electron.* **2014**, 20, 3802006 DOI: 10.1109/JSTQE.2014.2321517

[Crossref], [CAS]

9. 9.

Tsai, D. S.; Lien, W. C.; Lien, D. H.; Chen, K. M.; Tsai, M. L.; Senesky, D. G.; Yu, Y. C.; Pisano, A. P.;He, J. H. Solar-Blind Photodetectors for Harsh Electronics *Sci. Rep.* **2013**, 4, 2628 DOI: 10.1038/srep02628

[Crossref]

10. 10.

Lien, W. C.; Tsai, D. S.; Lien, D.-H.; Senesky, D. G.; He, J. H.; Pisano, A. P. 4H-SiC Metal-Semiconductor-Metal Ultraviolet Photodetectors in Operation of 450 °C *IEEE Electron Device Lett.* **2012**, 33, 1586– 1588DOI: 10.1109/LED.2012.2214759

[Crossref], [CAS]

11. 11.

Tsai, D. S.; Lin, C. A.; Lien, W. C.; Chang, H. C.; Wang, Y. L.; He, J. H. Ultra-High-Responsivity Broadband Detection of Si Metal-Semiconductor-Metal Schottky Photodetectors Improved by ZnO Nanorod Arrays *ACS Nano* **2011**, 5, 7748– 7753 DOI: 10.1021/nn203357e

[ACS Full Text], [CAS]

12. 12.

Trishenkov, M. A. *Detection of Low-Level Optical Signals: Photodetectors, Focal Plane Arrays and Systems*;Springer: New York, **1997**.

[Crossref]

13. 13.

Konstantatos, G.; Howard, I.; Fischer, A.; Hoogland, S.; Clifford, J.; Klem, E.; Levina, L.; Sargent, E. H.Ultrasensitive Solution-Cast Quantum Dot Photodetectors *Nature* **2006**, 442, 180– 183 DOI: 10.1038/nature04855

[Crossref], [PubMed], [CAS]

14. 14.

McDonald, S. A.; Konstantatos, G.; Zhang, S.; Cyr, P. W.; Klem, E. J. D.; Levina, L.; Sargent, E. H. Solution-Processed PbS Quantum Dot Infrared Photodetectors and Photovoltaics *Nat. Mater.* **2005**, 4, 138– 142 DOI: 10.1038/nmat1299

[Crossref], [PubMed], [CAS]

15. 15.

Dou, L.; Yang, Y.; You, J.; Hong, Z.; Chang, W. H.; Li, G.; Yang, Y. Solution-Processed Hybrid Perovskite Photodetectors with High Detectivity *Nat. Commun.* **2014**, 5, 5404 DOI: 10.1038/ncomms6404

[Crossref], [PubMed], [CAS]

16. 16.

Ma, C.; Shi, Y.; Hu, W.; Chiu, M. H.; Liu, Z.; Bera, A.; Li, F.; Wang, H.; Li, L. J.; Wu, T. Heterostructured $WS_2/CH_3NH_3PbI_3$ Photoconductors with Suppressed Dark Current and Enhanced Photodetectivity *Adv. Mater.* **2016**, 28, 3683– 3689 DOI: 10.1002/adma.201600069

[Crossref], [PubMed], [CAS]

17. 17.

Maculan, G.; Sheikh, A. D.; Abdelhady, A. L.; Saidaminov, M. I.; Haque, M. A.; Murali, B.; Alarousu, E.;Mohammed, O. F.; Wu, T.; Bakr, O. M. $CH_3NH_3PbCl_3$ Single Crystals: Inverse Temperature Crystallization and Visible-Blind UV-Photodetector *J. Phys. Chem. Lett.* **2015**, 6, 3781– 3786 DOI: 10.1021/acs.jpclett.5b01666

[ACS Full Text], [CAS]

18. 18.

Stolterfoht, M.; Armin, A.; Shoaee, S.; Kassal, I.; Burn, P.; Meredith, P. Slower Carriers Limit Charge Generation in Organic Semiconductor Light-Harvesting Systems *Nat. Commun.* **2016**, 7, 11944 DOI: 10.1038/ncomms11944

[Crossref], [PubMed], [CAS]

19. 19.

Tsai, M. L.; Wei, W. R.; Tang, L.; Chang, H. C.; Tai, S. H.; Yang, P. K.; Lau, S. P.; Chen, L. J.; He, J. H. Si Hybrid Solar Cells with 13% Efficiency *via* Concurrent Improvement in Optical and Electrical Properties by Employing Graphene Quantum Dots *ACS Nano* **2016**, 10, 815– 821 DOI: 10.1021/acsnano.5b05928

[ACS Full Text], [CAS]

20. 20.

Lin, C. A.; Tsai, M. L.; Wei, W. R.; Lai, K. Y.; He, J. H. Packaging Glass with a Hierarchically Nanostructured Surface: A Universal Method to Achieve Self-Cleaning Omnidirectional Solar Cells *ACS Nano* **2016**, 10,549– 555 DOI: 10.1021/acsnano.5b05564

[ACS Full Text], [CAS]

21. 21.

Wang, H. P.; Lin, T. Y.; Tsai, M. L.; Tu, W. C.; Huang, M. Y.; Liu, C. W.; Chueh, Y. L.; He, J. H. Toward Efficient and Omnidirectional n-Type Si Solar Cells: Concurrent Improvement in Optical and Electrical Characteristics by Employing Microscale Hierarchical Structures *ACS Nano* **2014**, 8, 2959– 2969 DOI: 10.1021/nn500257g

[ACS Full Text], [CAS]

22. 22.

Lin, G. J.; Wang, H. P.; Lien, D. H.; Fu, P. H.; Chang, H. C.; Ho, C. H.; Lin, C. A.; Lai, K. Y.; He, J. H. A Broadband and Omnidirectional Light-Harvesting Scheme Employing Nanospheres on Si Solar Cells *Nano Energy* **2014**, 6, 36– 43 DOI: 10.1016/j.nanoen.2014.03.004

[Crossref], [CAS]

23. 23.

Wang, H. P.; Lai, K. Y.; Lin, Y. R.; Lin, C. A.; He, J. H. Periodic Si Nanopillar Arrays Fabricated by Colloidal Lithography and Catalytic Etching for Broadband and Omnidirectional Elimination of Fresnel Reflection*Langmuir* **2010**, 26, 12855 DOI: 10.1021/la1012507

[ACS Full Text], [CAS]

24. 24.

Tsai, M. L.; Tu, W. C.; Tang, L.; Wei, T. C.; Wei, W. R.; Lau, S. P.; Chen, L. J.; He, J. H. Efficiency Enhancement of Silicon Heterojunction Solar Cells *via* Photon Management Using Graphene Quantum Dot as Downconverters *Nano Lett.* **2016**, 16, 309– 313 DOI: 10.1021/acs.nanolett.5b03814

[ACS Full Text], [CAS]

25. 25.

Mannheimer, P. D. The Light-Tissue Interaction of Pulse Oximetry *Anesth. Analg.* **2007**, 105, S10– S17 DOI: 10.1213/01.ane.0000269522.84942.54

[Crossref], [PubMed]

26. 26.

Tang, L.; Ji, R.; Cao, X.; Lin, J.; Jiang, H.; Li, X.; Teng, K. S.; Luk, C. M.; Zeng, S.; Hao, J.; Lau, S. P. Deep Ultraviolet Photoluminescence of Water-Soluble Self-Passivated Graphene Quantum Dots *ACS Nano* **2012**,6, 5102– 5110 DOI: 10.1021/nn300760g

[ACS Full Text], [CAS]

27. 27.

Oshima, C.; Nagashima, A. Ultra-Thin Epitaxial Films of Graphite and Hexagonal Boron Nitride on Solid Surfaces *J. Phys.: Condens. Matter* **1997**, 9, 1– 20 DOI: 10.1088/0953-8984/9/1/004

[Crossref], [CAS]

28. 28.

Liang, Z.; Zeng, P.; Liu, P.; Zhao, C.; Xie, W.; Mai, W. Interface Engineering To Boost Photoresponse Performance of Self-Powered, Broad-Bandwidth PEDOT:PSS/Si Heterojunction Photodetector *ACS Appl. Mater. Interfaces* **2016**, 8, 19158– 19167 DOI: 10.1021/acsami.6b06301

[ACS Full Text], [CAS]

29. 29.

Ferrari, M.; Quaresima, V. A Brief Review on the History of Human Functional Near-Infrared Spectroscopy (fNIRS) Development and Fields of Application *NeuroImage* **2012**, 63, 921– 935 DOI: 10.1016/j.neuroimage.2012.03.049

[Crossref], [PubMed], [CAS]

30. 30.

Shen, J.; Zhu, Y.; Chen, C.; Yang, X.; Li, C. Facile Preparation and Upconversion Luminescence of Graphene Quantum Dots *Chem. Commun.* **2011**, 47, 2580– 2582 DOI: 10.1039/C0CC04812G

[Crossref], [PubMed], [CAS]

31. 31.

Zhuo, S.; Shao, M.; Lee, S. T. Upconversion and downconversion Fluorescent Graphene Quantum Dots: Ultrasonic Preparation and Photocatalysis *ACS Nano* **2012**, 6, 1059– 1064 DOI: 10.1021/nn2040395

[ACS Full Text], [CAS]